Apparent breakdown of Raman selection rule at valley exciton resonances in monolayer MoS_2

Steven G. Drapcho,[1] Jonghwan Kim,[1] Xiaoping Hong,[1] Chenhao Jin,[1] Sufei Shi,[1,2,*]
Sefaattin Tongay,[3,†] Junqiao Wu,[2,3] and Feng Wang[1,2,4,‡]

[1]*Department of Physics, University of California at Berkeley, Berkeley, California 94720, USA*
[2]*Materials Science Division, Lawrence Berkeley National Laboratory, Berkeley, California 94720, USA*
[3]*Department of Materials Science and Engineering, University of California, Berkeley, California 94720, USA*
[4]*Kavli Energy NanoSciences Institute at the University of California, Berkeley and the Lawrence Berkeley National Laboratory, Berkeley, California 94720, USA*

(Received 12 January 2016; revised manuscript received 9 March 2017; published 13 April 2017)

The valley degree of freedom in atomically thin transition metal dichalcogenides (TMDCs) has generated great interest due to the possibility of using it to store and control information in analogy to the spin degree of freedom in spintronics. A signature of the valley pseudospin is the selective coupling of valley excitons to photons with defined helicity. This selectivity can have important consequences for a variety of optical phenomena associated with the valley excitons. Here we report that Raman features that seemingly violate the Raman selection rules can become prominent at valley exciton resonances in atomically thin MoS_2. Specifically, the Raman selection rule requires the excitation and scattering photons to have opposite circular polarizations for the in-plane E' mode phonon, but we observe an apparent E' Raman peak for excitation and scattered photons with the same circular polarization at exciton resonances. We attribute this peak to a defect-assisted process that involves phonons in the transverse optical E' branch slightly away from the Γ point, a process that can be enhanced by the selective coupling of valley pseudospin to photon helicity. Thus, the valley pseudospin, in addition to the crystal symmetry, may be important in understanding the Raman scattering spectra for excitations close to valley exciton resonances.

DOI: 10.1103/PhysRevB.95.165417

Atomically thin transition-metal dichalcogenides (TMDCs) have attracted significant attention as a promising platform for two-dimensional semiconductor nanoelectronics and nano-optics [1–12]. Due to a lack of inversion symmetry in monolayer TMDCs, the hexagonal Brillouin zone possesses a pair of degenerate but inequivalent valleys at the K and K' points [6]. This valley index or valley pseudospin serves as an additional electronic degree of freedom in addition to electron spin. Recently, it has been shown that the valleys can be manipulated selectively with circularly polarized light, raising the possibility of utilizing the valley pseudospin for quantum information applications [1–7]. This helicity-selective coupling between light and the valley degree of freedom can affect a variety of optical processes involving the valley excitons. Here we investigate its effect on Raman scattering. Raman spectroscopy has been used extensively on two-dimensional (2D) materials, such as graphene and TMDCs, for studying thickness-dependent properties [13–20] and probing strain effects [21,22]. However, few Raman studies have examined systematically the polarization selection rule for TMDCs with circularly polarized excitation and detection [23]. Here we perform polarization-resolved Raman spectroscopy on monolayers of MoS_2 with excitation wavelengths both on and off valley exciton resonance. We focus our analysis on the singly degenerate out-of-plane A_1' mode and the doubly degenerate in-plane E' mode, which arise from the A_{1g} mode and E^1_{2g} mode in bulk MoS_2, respectively [24]. Comparing our results to a group theory analysis based on the crystal symmetry, we observe that the A_1' mode always obeys the Raman selection rules. The E' mode, however, appears to violate the Raman selection rule at valley exciton resonances: it shows a prominent peak when the incoming and scattered light have the same circular polarization despite being forbidden by the Raman selection rule. We attribute the presence of this peak to a defect-assisted process involving E' phonons slightly away from the Γ point, which can be enhanced by the selective coupling of valley excitons to photon helicity at exciton resonances.

In our Raman measurements, we examine four different polarization configurations—the incoming and outgoing light having the same linear polarization, perpendicular linear polarization, same circular polarization, and opposite circular polarization (see Appendixes A and B for a description of the optical setup and sample preparation). Raman data were acquired for two laser excitation wavelengths: a 532 nm solid state laser and a 633 nm HeNe laser. Figure 1 shows the reflection difference spectrum in monolayer MoS_2, $(R_{sa} - R_{sb})/R_{sb}$, where R_{sa} is the reflection from the sample and R_{sb} is the reflection from the substrate. For a thin film, this reflection difference is directly proportional to the absorption [25,26]. We see that the 633 nm excitation is close to both the A exciton resonance at 655 nm and the B exciton resonance at 610 nm [8,10], so it corresponds to "on-resonance excitation" of the valley excitons. On the other hand, the 532 nm excitation is far away from both the A and B exciton peaks, so it corresponds to "off-resonance excitation" of the valley excitons. We note that the 532 nm light (2.33 eV) has energy higher than the monolayer MoS_2 exciton transition (1.9 eV), so it will be resonant with some interband transition [8,10].

*Current address: Department of Chemical and Biological Engineering, Rensselaer Polytechnic Institute, Troy, New York 12810, USA.
†Current address: School for Engineering of Matter, Transport and Energy, Arizona State University, Tempe, Arizona 85287, USA.
‡Correspondence to: fengwang76@berkeley.edu

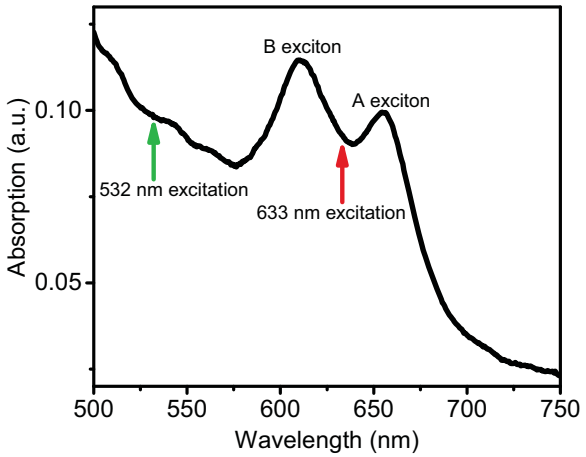

FIG. 1. The absorption spectrum of monolayer MoS_2 from a supercontinuum light source. The A and B exciton peaks at 655 and 610 nm are clearly visible. The laser excitation wavelengths at 633 and 532 nm used for polarization-resolved Raman measurements are labeled. The on-resonance 633 nm excitation is close to both the A and B exciton peaks, while the off-resonance 532 nm excitation is far from both exciton peaks.

We now examine our polarization-resolved Raman data for both laser excitation wavelengths (532 and 633 nm) for exfoliated monolayer MoS_2 on a Si/SiO_2 substrate. Figure 2(a) shows data for the off-resonance 532 nm excitation, and Fig. 2(b) shows data for the on-resonance 633 nm excitation. The data were acquired at room temperature. The spectral resolution of our Raman setup is around 8 cm^{-1}, limiting the sharpness of the Raman features we observe. We observe the prominent A_1' phonon mode at 408 rel. cm^{-1} and E' phonon mode at 388 rel. cm^{-1}, similar to those reported in earlier works [13,14]. The peak around 424 rel. cm^{-1} for the on-resonance 633 nm excitation is due to a second-order Raman process that is enhanced at exciton resonances and is mediated by exciton-polaritons [27,28]. The broad peak around 455 rel. cm^{-1} off-resonance is due to the second-order 2LA(M) mode, which involves two longitudinal acoustic phonons at the M point of the Brillouin zone, and the broad peak around 465 rel. cm^{-1} on-resonance has been previously assigned to a convolution of the 2LA(M) mode and phonons in the $A_{2u}(\Gamma)$ branch [27]. A strong background is also present in the on-resonance Raman spectra due to the tail of the photoluminescence peak in MoS_2. We find that additional polarization-resolved Raman measurements of CVD-grown MoS_2 [29] on a sapphire substrate show similar behavior to the exfoliated sample (see Appendix C).

For all polarization configurations and excitation wavelengths, the A_1' mode appears only when the incident and

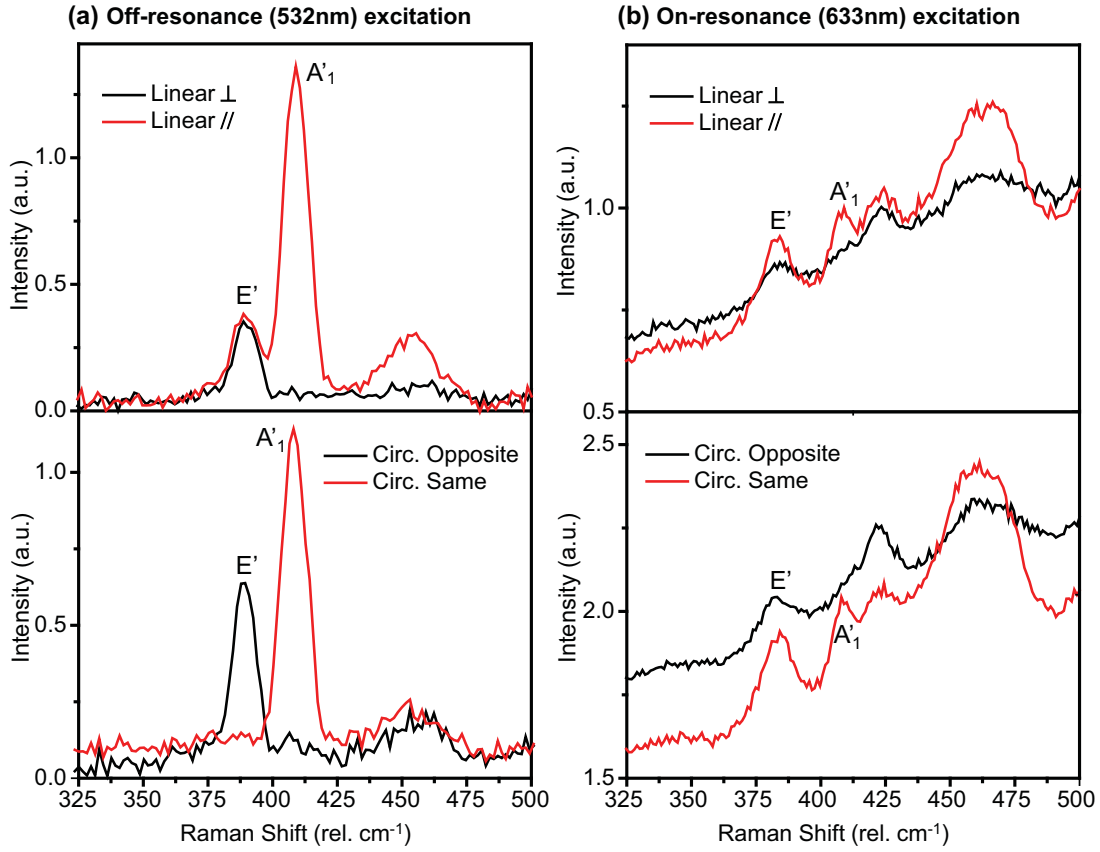

FIG. 2. Polarization-resolved Raman spectra for (a) off-resonance 532 nm excitation and (b) on-resonance 633 nm excitation of exfoliated monolayer MoS_2. The strong background on-resonance is from the tail of the MoS_2 photoluminescence peak. The A_1' mode at 408 rel. cm^{-1} exhibits the same selection rule for both on- and off-resonance excitations. The E' mode at 388 rel. cm^{-1} is absent for the circular same polarization off-resonance, but seems to appear on-resonance. The additional peaks in the spectra are mostly due to multiphonon processes and have been identified in previous studies [25].

outgoing light have the same linear or circular polarizations. The behavior of E' mode, however, appears to be different for the excitations on and off the valley exciton resonances. For the off-resonance excitation, the E' mode is present when the incident and backscattered photons have opposite circular polarizations, and it is absent when the incident and backscattered photon have the same circular polarization. For the on-resonance excitation, however, the E' mode shows a prominent Raman peak when the incident and backscattered photons have the same circular polarization. With linearly polarized excitation, the E' mode always appears for both parallel and perpendicular linear polarization configurations. Additionally, the E' mode appears to redshift by around 3 rel. cm^{-1} in the on-resonant excitation compared to the off-resonant excitation, which will be discussed further in the following.

To understand this unusual circular polarization-dependent Raman scattering in MoS_2, we first examine the Raman scattering selection rules arising from the crystal symmetry using a group theory analysis. The Raman scattering cross section for a given incident and scattered light polarization and a given phonon mode is proportional to $|\langle \hat{e}_i | \boldsymbol{R} | \hat{e}_o \rangle|^2$, where $\hat{e}_i$ and $\hat{e}_o$ are the polarization vectors of the incoming and outgoing light, and R is the Raman tensor for the phonon mode under consideration [30,31]. If the Raman cross section is required to be zero by symmetry, the mode is forbidden, otherwise it is allowed. In a first-order Raman process, an electron can be thought of as absorbing a photon, scattering with a phonon, and emitting a photon to return to its initial state. Since the initial and final states of the electron are the same, the wave vector difference of the incident and emitted light must be equal to the wave vector of the phonon mode involved. The wave vectors of the light are very small compared to the size of the Brillouin zone, so for normal incident and backscattered light, the phonons that can contribute to a first-order Raman process must also have a wave vector near the Γ point. The Brillouin zone center has the same symmetry as the lattice, so each Γ point phonon mode must transform as one of the irreducible representations of the point group of the lattice. The irreducible representation of a phonon mode determines the form of its Raman tensor [30,31], i.e., which elements are required to be zero and which may not be zero. Once the Raman tensor is known, the Raman scattering cross section can be evaluated for a given set of ingoing and outgoing light polarizations.

The crystal structure of monolayer MoS_2 belongs to the symmetry point group D_{3h} [24]. For this point group and with normally incident light, the only modes that can play a role in first-order Raman scattering are the doubly degenerate E' and singly degenerate A_1' modes [24]. Therefore, we focus on the E' and A_1' modes in our analysis. Figure 3(a) shows a schematic of the atomic displacements of the Mo and S atoms for these modes. In writing down the Raman tensors and light polarization vectors, we neglect the out-of-plane z component because for normally incident and backscattered light the polarization directions will lie in the plane of the material and only the in-plane symmetry of the material matters. We use circularly polarized light as our basis, where the polarization vector for right circularly polarized light is (1,0) and left circularly polarized light is (0,1). In this basis, linearly polarized light in the x direction can be written as $(1/\sqrt{2})^*(1,1)$ and linearly polarized light in the y direction

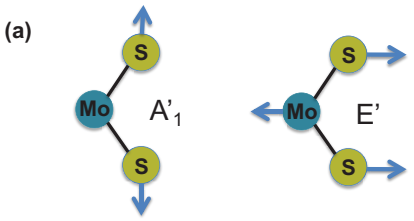

(b)

	Linear //	Linear ⊥	Circ. Same	Circ. Opposite
E' theory	O	O	**X**	O
A'_1 theory	O	X	O	X
E' exp.	O	O	**O**	O
A'_1 exp.	O	X	O	X

FIG. 3. (a) A schematic of the atomic vibrations for the A_1' and E' phonon modes in monolayer MoS_2. **(b)** The group theoretical selection rules and the experimental data for the polarization-resolved Raman measurements. "O" indicates that a mode is allowed (theory) or observed (experiment), and "X" indicates that a mode is forbidden (theory) or absent (experiment). The colored and bolded **X** and **O** highlight where the experimental data seems to conflict with the theoretical selection rule.

can be written as $(1/\sqrt{2})^*(1,-1)$. The singly degenerate A_1' mode involves only vibrations in the z direction, so it cannot alter the polarization of light in the x or y directions during Raman scattering. With our coordinate system, the Raman tensor for the A_1' mode is $\left[\begin{smallmatrix} a & 0 \\ 0 & a \end{smallmatrix}\right]$. On the other hand, the doubly degenerate E' mode involves in-plane atomic vibrations, which can alter the polarization of light in the x and y directions. The Raman tensors for the two degenerate E' modes can be written as $\left[\begin{smallmatrix} 0 & b \\ 0 & 0 \end{smallmatrix}\right]$ and $\left[\begin{smallmatrix} 0 & 0 \\ b & 0 \end{smallmatrix}\right]$, respectively. We can now calculate which polarization configurations are forbidden and which are allowed for each phonon mode. Figure 3(b) shows a table of the calculated Raman selection rules for the A_1' and E' modes for each polarization configuration, with "O" denoting that a polarization configuration is allowed for a given phonon mode, and "X" denoting that it is forbidden.

We can also gain a physical understanding of the selection rules by considering the threefold rotational symmetry of the lattice. For a crystal potential that is periodic in space, Bloch's theorem and the crystal boundary conditions lead to discretized values of momentum that are conserved up to a reciprocal lattice vector $\boldsymbol{G}$, where $\boldsymbol{G}$ connects two reciprocal lattice points. Analogously, for a lattice with threefold rotational symmetry, an angular momentum with discretized values can be introduced, and the total angular momentum is conserved up to multiples of $3\hbar$ since a rotation by $2\pi/3$ maps the lattice onto itself. The A_1' phonon mode transforms like the function x^2+y^2, which corresponds to zero angular momentum [28]. As a result, it can only couple two photons with the same angular momentum. The two E' phonons transform like $(x+iy)^2$ and $(x-iy)^2$, which correspond to an angular momentum of $2\hbar$ and $-2\hbar$, respectively [28]. The $(x \pm iy)^2$ phonons can couple an incident photon with angular

momentum $\mp\hbar$ to a scattered photon with angular momentum $\pm\hbar$. However, they cannot couple photons with the same angular momentum. Therefore, the crystal symmetry forbids the E' mode from Raman scattering where the incident and scattered light have the same circular polarization.

We now compare our data to the selection rules obtained from group theory, which are tabulated in Fig. 3(b). We see that for the A_1' mode, our data for all polarization configurations and excitation wavelengths agree with the Raman selection rules. For the E' mode, however, the behavior is different. The Raman selection rule is satisfied for the off-resonance excitation, but it is seemingly violated when the excitation is at the valley exciton resonances: the E' mode shows a prominent peak for the same circular ingoing and outgoing configuration even though it should be forbidden.

To understand our result, we need to consider both the phonon bands and the optical properties of valley excitons in monolayer MoS_2. First, we examine the phonon band structure to explain the 3 rel. cm^{-1} redshift we observe for the E' mode on-resonance. Examining the calculated energies of the phonons at high-symmetry points in monolayer MoS_2, we see that there is no second-order process involving phonons at the Γ or M points that has an energy within a few rel. cm^{-1} of the E' phonon mode [32,33]. Additionally, the transverse optical E' branch becomes lower in energy for k values slightly away from the Γ point. In a normal first-order Raman process, the phonons involved must have effectively zero momentum. On exciton resonance, however, the real exciton states excited by the incident light can interact with defects, which can provide the additional momentum needed to emit a phonon with a small but finite wave vector. Thus, we believe that the slight redshift we observe for the E' mode on-resonance arises from a defect-assisted process involving phonons in the transverse optical E' branch slightly away from the Γ point and not a second-order combination of phonons from the Γ or M points. Qualitatively similar on-resonance Raman spectra were observed in Ref. [27] for single-layer and few-layer MoS_2 without polarization resolution, and the behavior of the E' peak was also attributed to phonons in the E' branch slightly away from $k = 0$. We note that the behavior we observe did not seem to appear prominently in the helicity-resolved Raman scattering measurements performed in Ref. [23], which may be due to a lower concentration of defects in the samples used by Ref. [23].

Now we consider the helicity of the valley excitons to address the polarization dependence we observe. Polarization-resolved photoluminescence measurements have shown previously that a given valley preferentially absorbs and emits light of the same circular polarization [1,4,6,7]. Thus, for on-resonance excitation with circularly polarized photons, one valley exciton will be preferentially excited. In first-order Raman processes the momentum of the light and phonon involved is very small compared to the Brillouin zone, so the exciton will remain in the same valley after emitting a phonon and cannot scatter to the other valley. This remains true for phonons slightly away from the Γ point that we believe are responsible for the E' peak we observe in the same circular polarization configuration. The Raman selection rule arising from the crystal symmetry will not be completely strict for phonons with a small but finite momentum. Therefore, the valley circular polarization selectivity will favor Raman processes with the incident and outgoing photons having the same circular polarization and suppress the circular opposite configuration, in competition with the Raman selection rule that favors the opposite behavior.

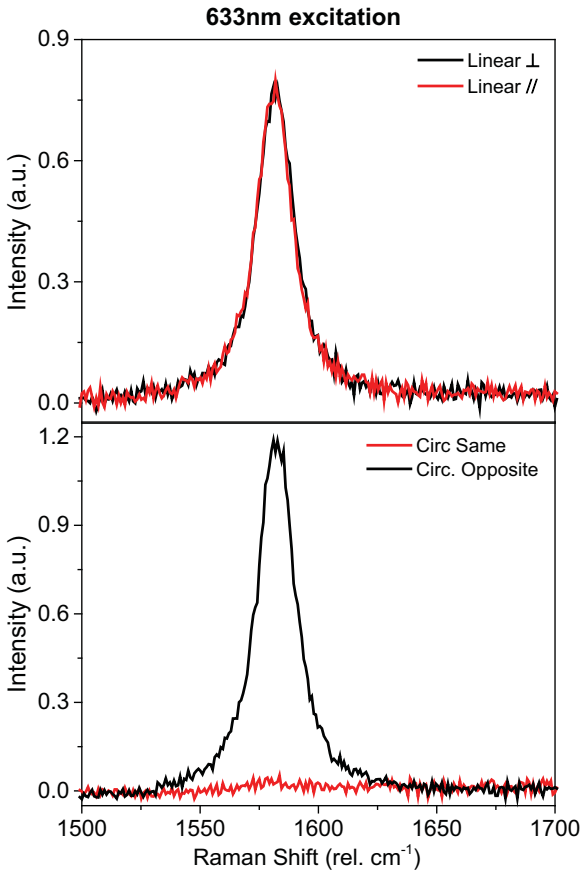

FIG. 4. Polarization-dependent Raman spectra for the G mode in graphene. The Raman selection rules for the G mode in graphene, a system with no selective coupling of valley pseudospin to photon helicity, are identical to those of the E' mode in monolayer MoS_2. For the 633 nm excitation, we see that the G mode obeys these selection rules.

To rule out the possibility that our observation of phonons in the E' branch for the same circular polarization case is due to polarization impurity from our polarization optics, we measure the extinction ratio of the total reflected light from the sample in our Raman setup for the linear polarization geometries and the circular polarization geometries. For the 532 nm excitation, the extinction ratios we measure ($I_{\text{linear parallel}}/I_{\text{linear perpendicular}}$ and $I_{\text{circular same}}/I_{\text{circular opposite}}$, where I denotes intensity) are 29 000 and 145, respectively, and for the 633 nm excitation, the same extinction ratios are 7800 and 6000, respectively. This indicates that our observation of the E' mode for the circular parallel configuration for the on-resonance 633 nm excitation is not due to an artifact from polarization impurity.

We also perform a control measurement with the 633 nm excitation on the G mode in exfoliated monolayer graphene (see Fig. 4), which has identical Raman selection rules to the E' mode in monolayer MoS_2 [22]. The Raman spectra we observe for the G mode in graphene, a system with no valley polarization, exactly obey these selection rules, indicating that

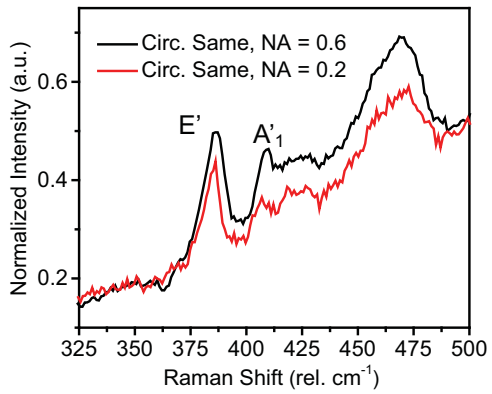

FIG. 5. Raman spectra for monolayer exfoliated MoS_2 for two different numerical apertures (NAs) for the incident and scattered light having the same circular polarization. Each spectrum is normalized by the maximum of the photoluminescence peak. Reducing the NA does not affect the presence of the E' mode, indicating that in-plane photon momentum likely does not play a large role in the apparent violation of the Raman selection rule for the E' phonon mode.

the seeming violation of the E' mode we observe in MoS_2 is due to an effect in that system that is not present in graphene. In graphene, it is known that the appearance of the G mode in Raman spectra relies on trigonal warping of the electronic states in the Dirac cone involved in the Raman scattering process [34,35]. Without trigonal warping, the electronic states would be isotropic and lack threefold rotational symmetry, forbidding the G mode in any polarization configuration [34,35]. Similarly, in MoS_2, the valley exciton states are isotropic in the absence of trigonal warping. However, trigonal warping in MoS_2 is stronger than that present in graphene [36,37], so the selection rules arising from the crystal symmetry should still apply to Raman scattering involving the real valley exciton electronic states excited on-resonance.

In addition, we test the effect of in-plane photon momentum by measuring Raman spectra of exfoliated MoS_2 with different numerical aperture of the laser excitation and light collection (Fig. 5). In the case of Fröhlich coupling, it is known that resonance excitation can enhance Raman-forbidden processes through coupling to finite-momentum bulk polar phonons, and the strength of this coupling depends strongly on the in-plane phonon wave number [38,39]. We find that the Raman spectra shape does not change significantly, indicating that in-plane photon momentum does not play a large role.

Our analysis shows that on-resonance Raman scattering of phonons in the E' branch near the Brillouin zone center in atomically thin TMDCs like MoS_2 may be strongly affected by two competing factors: the Raman selection rule from the crystal symmetry favors Raman scattering with opposite incident and scattered circular polarizations, while the valley exciton selectivity favors the same incident and scattered circular polarizations. Our experiment suggests that these two competing factors can have comparable effects on the E' mode Raman intensity in MoS_2, as we observe E' phonon peaks of comparable intensities for same and opposite circular polarization configurations. Thus, the valley degree of freedom can be important along with the crystal symmetry for determining the Raman spectra for on-resonance excitations.

This work was primarily supported by Office of Basic Energy Science, U.S. Department of Energy under Contract No. DE-AC02-05CH11231 (van der Waals heterostructure program). S.G.D. acknowledges support by the Department of Defense (DoD) through the National Defense Science & Engineering Graduate Fellowship (NDSEG) Program. The authors thank Yuen-Ron Shen for helpful discussions.

S.G.D., J.K., and X.H. contributed equally to this work.

APPENDIX A: DESCRIPTION OF OPTICAL MEASUREMENTS

Raman spectroscopy was performed with a confocal microscopy setup with the capability to image the sample and perform Raman measurements, as shown in Fig. 6. All measurements were done with normally incident laser light, with the backscattered light collected for detection. An initial polarizer sets the linear polarization of the incident light, and a polarizer before the detector controls the polarization of the measured light. The polarizer before the detector is left unchanged for all configurations, eliminating variation due to polarization-dependent detection efficiency from the spectrometer and detector. For the linear polarization configurations, a half-wave plate in the path of the outgoing light controls which linear polarization is detected. For the circular polarization configurations, an additional quarter-wave plate before the sample circularly polarizes the incident light and the half-wave plate controls which circular polarization is detected. A liquid nitrogen-cooled silicon CCD camera coupled to a monochrometer was used for detection.

Inset: An optical microscope image of the exfoliated monolayer MoS_2 flake used for Raman measurements. The scale bar is 15 μm.

For the absorption measurement, monolayers of MoS_2 were grown with chemical-vapor deposition (CVD) and transferred onto a sapphire substrate. The measurement was performed with a confocal microscopy setup using a broadband supercontinuum laser as the light source and a spectrometer

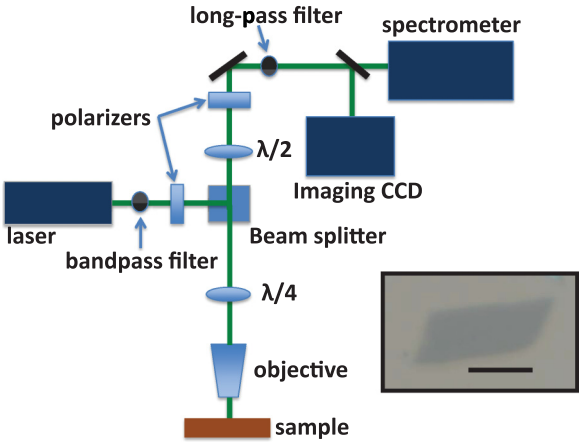

FIG. 6. Schematic of experimental setup used for polarization-resolved Raman measurements.

equipped with a one-dimensional CCD array for detection of the reflected light. The reference spectrum R_{sb} was taken on the sapphire substrate near the sample.

APPENDIX B: SAMPLE PREPARATION

Monolayers of exfoliated MoS_2 and exfoliated graphene were prepared by standard micromechanical exfoliation techniques and identified with optical contrast in a microscope. Figure 6 inset shows an optical microscope image of the exfoliated MoS_2 monolayer used for Raman measurements on a Si/SiO_2 substrate with 300 nm SiO_2 thickness.

CVD MoS_2 monolayers were grown onto *c*-cut sapphire substrates using the ambient pressure vapor transport technique. Sapphire samples were etched in piranha solution for 3 h at 65 °C and washed in DI water multiple times. Growth was performed in a two-zone furnace using semiconductor grade sulfur (access amount ~100 mg) and MoO_3 powders (4 mg). Samples were placed 1 cm directly above MoO_3 powders and the sulfur to reaction chamber distance was kept at 20 cm. The sulfur gas [S_2(g)] was carried by high-purity N_2 gas at a flowrate of 10 sccm. We notice that the temperature at which S_2(g) passes is of paramount importance to have ultimate control over domain size, shape, quality, and continuity. Typically, S_2(g) was passed above 590 °C and the growth was performed at 665 °C (at the reaction spot). During growth the flow rate was adjusted down to 3 sccm to improve the overall monolayer quality and improve continuity of monolayers. Growth duration was fixed at 5 min and samples were cooled down to 550 °C at a rate of 30 °C/min and fast cooled between 550−20 °C.

APPENDIX C: POLARIZATION-RESOLVED RAMAN SPECTRA OF CVD-GROWN MoS_2

Figure 7 shows polarization-resolved Raman spectra for (a) off-resonance 532 nm excitation and (b) on-resonance 633 nm excitation of CVD-grown monolayer MoS_2 on a sapphire substrate. The Raman spectra here show the same behavior as the exfoliated monolayer MoS_2 in the main text in Fig. 2. The strong background on-resonance is from the tail of the MoS_2 photoluminescence peak. The A_1' mode at 408 rel. cm^{-1} exhibits the same behavior for both on- and off-resonance excitations and always obeys the Raman selection rules. The E' mode at 388 rel. cm^{-1} is absent for the circular same polarization off-resonance, but appears on-resonance in apparent contradiction to the Raman selection rule. The additional peaks in the spectra are due to multiphonon processes as described in the main text.

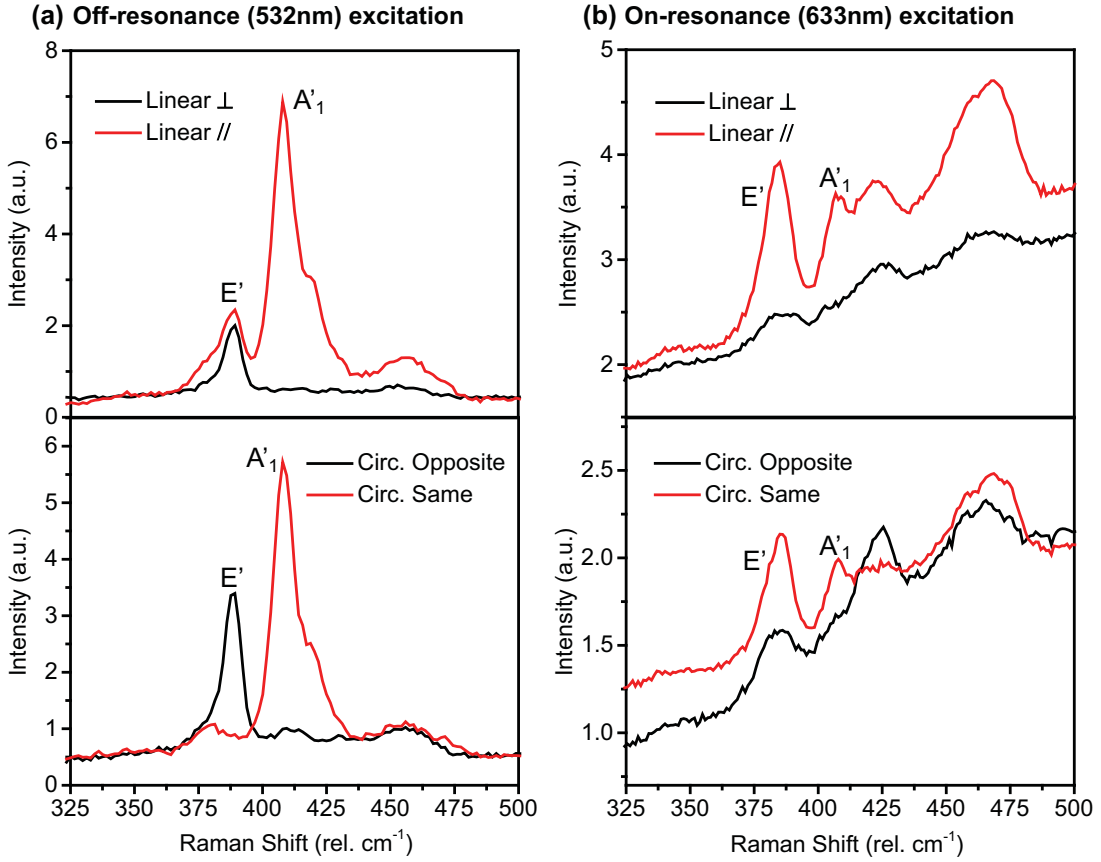

FIG. 7. Polarization-resolved Raman spectra of CVD-grown MoS_2.

[1] T. Cao, G. Wang, W. Han, H. Ye, C. Zhu, J. Shi, Q. Niu, P. Tan, E. Wang, B. Liu, and J. Feng, Nat. Commun. **3**, 887 (2012).

[2] J. Kim, X. Hong, C. Jin, S. Shi, C. Y. S. Chang, M. H. Chiu, L. J. Li, and F. Wang, Science **346**, 1205 (2014).

[3] K. F. Mak, K. L. McGill, J. Park, and P. L. McEuen, Science **344**, 1489 (2014).

[4] K. F. Mak, K. He, J. Shan, and T. F. Heinz, Nat. Nanotechnol. **7**, 494 (2012).

[5] E. J. Sie, J. W. McIver, Y. H. Lee, L. Fu, J. Kong, and N. Gedik, Nat. Mater. **14**, 290 (2014).

[6] D. Xiao, G. B. Liu, W. Feng, X. Xu, and W. Yao, Phys. Rev. Lett. **108**, 196802 (2012).

[7] H. Zeng, J. Dai, W. Yao, D. Xiao, and X. Cui, Nat. Nanotechnol. **7**, 490 (2012).

[8] K. F. Mak, C. Lee, J. Hone, J. Shan, and T. F. Heinz, Phys. Rev. Lett. **105**, 136805 (2010).

[9] B. Radisavljevic, A. Radenovic, J. Brivio, V. Giacometti, and A. Kis, Nat. Nanotechnol. **6**, 147 (2011).

[10] A. Splendiani, L. Sun, Y. Zhang, T. Li, J. Kim, C. Y. Chim, G. Galli, and F. Wang, Nano Lett. **10**, 1271 (2010).

[11] Q. H. Wang, K. Kalantar-Zadeh, A. Kis, J. N. Coleman, and M. S. Strano, Nat. Nanotechnol. **7**, 699 (2012).

[12] F. Xia, H. Wang, D. Xiao, M. Dubey, and A. Ramasubramaniam, Nat. Photon. **8**, 899 (2014).

[13] Y. Zhao, X. Luo, H. Li, J. Zhang, P. T. Araujo, C. K. Gan, J. Wu, H. Zhang, S. Y. Quek, M. S. Dresselhaus, and Q. Xiong, Nano Lett. **13**, 1007 (2013).

[14] X. Zhang, W. P. Han, J. B. Wu, S. Milana, Y. Lu, Q. Q. Li, A. C. Ferrari, and P. H. Tan, Phys. Rev. B **87**, 115413 (2013).

[15] H. Sahin, S. Tongay, S. Horzum, W. Fan, J. Zhou, J. Li, J. Wu, and F. M. Peeters, Phys. Rev. B **87**, 165409 (2013).

[16] C. Lee, H. Yan, L. E. Brus, T. F. Heinz, J. Hone, and S. Ryu, ACS Nano **4**, 2695 (2010).

[17] A. Berkdemir, H. R. Gutiérrez, A. R. Botello-Méndez, N. Perea-López, A. L. Elías, C. I. Chia, B. Wang, V. H. Crespi, F. López-Urías, J. C. Charlier, H. Terrones, and M. Terrones, Sci. Rep. **3**, 1755 (2013).

[18] X. Luo, Y. Zhao, J. Zhang, M. Toh, C. Kloc, Q. Xiong, and S. Y. Quek, Phys. Rev. B **88**, 195313 (2013).

[19] N. Scheuschner, R. Gillen, M. Staiger, and J. Maultzsch, Phys. Rev. B **91**, 235409 (2015).

[20] G. Froehlicher, E. Lorchat, F. Fernique, C. Joshi, A. Molina-Sánchez, L. Wirtz, and S. Berciaud, Nano Lett. **15**, 6481 (2015).

[21] H. J. Conley, B. Wang, J. I. Ziegler, R. F. Haglund, S. T. Pantelides, and K. I. Bolotin, Nano Lett. **13**, 3626 (2013).

[22] T. M. G. Mohiuddin, A. Lombardo, R. R. Nair, A. Bonetti, G. Savini, R. Jalil, N. Bonini, D. M. Basko, C. Galiotis, N. Marzari, K. S. Novoselov, A. K. Geim, and A. C. Ferrari, Phys. Rev. B **79**, 205433 (2009).

[23] S. Y. Chen, C. Zheng, M. S. Fuhrer, and J. Yan, Nano Lett. **15**, 2526 (2015).

[24] J. Ribeiro-Soares, R. M. Almeida, E. B. Barros, P. T. Araujo, M. S. Dresselhaus, L. G. Cançado, and A. Jorio, Phys. Rev. B **90**, 115438 (2014).

[25] F. Wang, Y. Zhang, C. Tian, C. Girit, A. Zettl, M. Crommie, and Y. R. Shen, Science **320**, 206 (2008).

[26] K. F. Mak, M. Y. Sfeir, Y. Wu, C. H. Lui, J. A. Misewich, and T. F. Heinz, Phys. Rev. Lett. **101**, 196405 (2008).

[27] J. U. Lee, J. Park, Y. W. Son, and H. Cheong, Nanoscale **7**, 3229 (2015).

[28] K. Gołasa, M. Grzeszczyk, P. Leszczyński, C. Faugeras, A. A. L. Nicolet, A. Wysmołek, M. Potemski, and A. Babiński, Appl. Phys. Lett. **104**, 092106 (2014).

[29] A. M. van der Zande, P. Y. Huang, D. A. Chenet, T. C. Berkelbach, Y. You, G. H. Lee, T. F. Heinz, D. R. Reichman, D. A. Muller, and J. C. Hone, Nat. Mater. **12**, 554 (2013).

[30] P. Yu and M. Cardona, *Fundamentals of Semiconductors: Physics and Material Properties* (Springer, Berlin, 2010).

[31] M. Dresselhaus, G. Dresselhaus, A Jorio, and V. Heine, *Group Theory: Application to the Physics of Condensed Matter* (Springer, Berlin, 2008).

[32] T. Livneh and J. E. Spanier, 2D Mater. **2**, 035003 (2015).

[33] A. Molina-Sanchez and L. Wirtz, Phys. Rev. B **84**, 155413 (2011).

[34] D. M. Basko, New J. Phys. **11**, 095011 (2009).

[35] P. Kossacki, C. Faugeras, M. Kuhne, M. Orlita, A. A. L. Nicolet, J. M. Schneider, D. M. Basko, Yu. I. Latyshev, and M. Potemski, Phys. Rev. B **84**, 235138 (2011).

[36] A. Kormanyos, V. Zolyomi, N. D. Drummond, P. Rakyta, G. Burkard, and V. I. Fal'ko, Phys. Rev. B **88**, 045416 (2013).

[37] H. Rostami, A. G. Moghaddam, and R. Asgari, Phys. Rev. B **88**, 085440 (2013).

[38] P. J. Colwell and M. V. Klein, Solid State Commun. **8**, 2095 (1970).

[39] R. M. Martin, Phys. Rev. B **4**, 3676 (1971).